Available online at https://ganitjournal.bdmathsociety.org/

GANIT: Journal of Bangladesh Mathematical Society

GANIT *J. Bangladesh Math. Soc.* 44.2 (2024) 047–064
DOI: https://doi.org/10.3329/ganit.v44i2.78532

Application of Finite Element Method to Problems with Mixed Boundary Conditions

Sadia Akter Lima [*1], Kamrunnesa Mayeda[2], Amin Ullah[3], and Md. Kamrujjaman[4]

[1, 2, 3] *Department of Applied Mathematics, Noakhali Science and Technology University, Noakhali-3814, Bangladesh*
[4] *Department of Mathematics, University of Dhaka, Dhaka-1000, Bangladesh*

ABSTRACT

In this study, we explore the effectiveness of the Finite Element Method (FEM) employing linear shape functions to address problems governed by Dirichlet, Neumann, and Robin boundary conditions. We use the derived weak formulation of FEM to solve various types of partial differential equations (PDEs) with mixed boundary conditions. Convergence and stability analyses are carried out to evaluate the performance of this approach, and different types of errors, like absolute error, dissipation, dispersion, and total mean square error, are investigated. This method is applied, and both the exact and approximate solutions are tabulated in three distinct cases: a one-dimensional Burgers-Huxley equation with Dirichlet boundary conditions; a diffusion-reaction equation with Neumann boundary conditions; and a uniformly propagating shock problem with Robin boundary conditions. Approximate solutions are compared to exact ones through 2D and 3D graphical representations, and tabular data offers a thorough error analysis. Additionally, error maps provide strong evidence for the accuracy of the suggested approach, demonstrating its capacity to precisely and quickly solve challenging problems with a variety of boundary conditions.

Received: October 11, 2024 **Accepted:** November 07, 2024 **Published Online:** December 30, 2024

Keywords: Finite Element Method; Shape Functions; Mixed Boundary Conditions; Convergence and Stability Analysis; Error Analysis;
AMS Subject Classification: 65N30, 35K20, 65N12, 65N15, 65N30.

1 Introduction

In many important fields, such as engineering, applied mathematics, and physics, the FEM is a powerful numerical tool that is used to handle complicated problems that are very challenging to understand theoretically. This renowned approach acts effectively for problems with complex geometries, a variety of boundary conditions, and heterogeneous materials. In this study, we explore how to apply the FEM with linear shape functions to Dirichlet, Neumann, and Robin boundary condition problems. When the value of the dependent variable, like temperature or displacement, at the boundary is known, then it is specified as a Dirichlet boundary condition. Conversely, when the value of the dependent variable's normal derivative is known at the boundary, then it is

*E-mail: sadia.amath@nstu.edu.bd, Phone: +880 1701451426

specified as a Neumann boundary condition. Furthermore, a linear relationship between the dependent variable and its normal derivative at the boundary and a combination of the Dirichlet and Neumann requirements is specified as a Robin boundary condition. The piecewise polynomial interpolation theory, on which the whole domain is divided into a finite number of elements and the behavior of each element is characterized by a system of elementary equations, is the fundamental idea of the FEM. A detailed explanation of the FEM was provided in [1], and a MATLAB solution for this method was covered in [2]. A weak Galerkin finite element technique for Oseen equations in incompressible fluid flow was proposed by C. Zhangxin [3], employing weak gradient and divergence operators for discontinuous functions. Numerical experiments demonstrated strong accuracy and stability of the approach, together with reduced degrees of freedom and increased flexibility. The finite element analysis approach, which is a tool used in the nuclear and aerospace industries to approximate challenging problem solutions, was thoroughly explained by the author of [4]. The study [5] included a detailed discussion of heat transfer, fluid mechanics, structural mechanics, and other non-linear analytical concepts. For time fractional PDEs, the authors of [6] examined the FEM using the Lax-Milgram Lemma to prove the existence and uniqueness of solutions. They also proposed a time-based step approach and developed optimal convergence and error calculations. In the framework of non-linear parabolic PDEs with Robin boundary conditions, H. Ali and M. Kamrujjaman [7] explored the Galerkin Finite Element Method (GFEM) approximation of classical solutions. They examined the convergence, uniqueness, and structural stability of a solution. Additionally, a comparison between the exact and approximate solutions verified the accuracy and effectiveness of the method. [8] provided examples of how it estimated convergence and stability, computed error, and resolved challenging problems such as the Fisher, Newell-Whitehead-Segel, Burger, and Burgers-Huxley equations. These examples showed its applicability, simplicity, accuracy, and efficiency. In [9], it was introduced four iterative methods for solving non-linear equations: Broyden's method (BM), optimal fourth-order method (OFOM), optimal sixth-order method (OSOM), and homotopy continuation method (HCM). The methods were compared using real-world models, and their effectiveness was demonstrated by numerical analysis [9]. Which technique is better was determined by the study [9] based on specific features. For the purpose of numerically solving the fractional-order Bagley-Torvik equation of order (0, 2), the authors of [10] presented a new methodology that was based on the currently used FEM. The approach was simple, generalizable, and provided clear, concise, and accurate results. The methodology yielded the same solution path for comparable fractional-order boundary value problems and beat current approaches that used a restricted set of quadratic functions. Using the GFEM, the FitzHugh-Nagumo equation was numerically solved in [11]. A generalized Burgers' and Fisher's equation—an advection-diffusion-reaction equation in two dimensions of space—was examined in the paper [12]. It produced positive and limiting solutions by proposing an exact finite-difference discretization of the Burgers-Fisher model. It was a positivistic, bounded, monotonic technique that converged with first order in time and second order in space. [13] described a new algorithm for solving two-dimensional non-linear Burgers-Huxley equations. The approach was precise and high-order compact, and it produced high-order precision within a smooth flow zone. It was stable and accurate up to two orders in time and six orders in space. The efficiency was described in terms of L_2 and L_∞ norms, and the proposed methods could be used to address real-world problems in science and engineering. In [14], PDEs were presented and classified with a focus on their applications in science and engineering. We also discussed the possible numerical methods for solving these equations. [15] provided a mathematical framework for a posteriori error estimates of finite element solutions using bilinear forms on Hilbert spaces. The primary theorem gave an optimal estimate with equal upper and lower error bounds. Furthermore, the theory suggested adaptive mesh refinement strategies and performed well in numerical instances. For finite element processes applied to boundary value problems (BVPs) using self-adjoint, non-self-adjoint, and non-linear differential operators, the study [16] derived a priori and a posteriori error estimates. It placed emphasis on local approximations and variational consistency in higher-order scalar product spaces, allowing for precise convergence rate analysis and error computation regardless of the approximation technique. A two-step Lax-Wendroff type detection scheme with phase characteristics and accuracy similar to third-order schemes was derived by the author in [17]. The method was exactly third-order correct in time and space for uniform flow. When it comes to simulating the advection of localized shocks with steep gradients, the suggested strategy fared better than earlier methods. Originally designed for continuous flow, the plan was later extended to include nonuniform two-dimensional flow. Nonstandard, Euler finite difference, and unconditionally positive

schemes were numerically investigated in [18] to solve non-linear convection-diffusion-reaction equations. Von-Neumann stability analysis was used to explore stability, consistency, and spectrum analysis. The effectiveness of the different approaches was put to the test numerically. The collocation approach provided a numerical solution to the Burgers-Huxley equation using the cubic B-spline as the basis function. The Crank-Nicolson implicit methodology was used to discretize and quasi-linearize the procedure in [19]. The study [20] created finite-dimensional dynamics for the classical Burgers-Huxley problem using evolutionary PDEs, and then they created new precise solutions. The [21] study used the Padé Approximation approach to numerically solve the Helmholtz equation, an issue that arose in a variety of domains. The equation was backed into power series after being transformed into Padé series form. The Homotopy Perturbation Method (HPM) was used in [22] to describe a one-dimensional heat equation with Neumann and Dirichlet starting boundary conditions. HPM was a potent mathematical tool that yielded continuous replies and extremely accurate findings. The FEM was used by S. A. Lima et al. [23] to study the numerical approximation of non-linear parabolic PDEs. By using small time step sizes, it sought to determine the acceptability and correctness of the mentioned method by solving Fisher's equation and the FitzHugh-Nagumo equation using regular and irregular geometrical shapes. The convection-diffusion-reaction (CDR) equation's numerical approximations were found in [24] using the FEM. It analyzed the convergence and stability of non-linear PDEs and looked at both regular and irregular geometric shapes. The study used dissipation error, dispersion error, and total error analysis to ensure technique validity and efficiency. S. A. Lima and F. Khondaker [25] examined the FEM to assess 2D higher-order non-homogeneous diffusion-reaction equations more precisely. To ensure the reliability and efficiency of the FEM, they employed both regular and irregular geometric shapes in addition to absolute error analysis. In [26], GFEM was utilized to address non-linear boundary value problems of second order. The accuracy, compatibility, and applicability of the system were demonstrated by this study, which also provided a generalized formulation and discovered approximations for a few problems.

The significance of FEM in the realm of numerical analysis may become clear to us after reading the comments provided above. At each nodal point, the FEM may exhibit a good agreement with the properties of an exact solution, making it a superior choice for obtaining a more accurate solution with stability and higher order convergence. The authors of [23]–[26] employed a straightforward FEM formulation with two linear shape functions, which can quickly and readily compute more accurate solutions for complex issues. They did not provide a special formulation that works with both Neumann and Robin boundary conditions, instead concentrating on solving both linear and nonlinear CDR equations with Dirichlet boundary conditions. In numerical simulations and mathematical modeling, both the numerical value and the rate of change are essential to forming these conditions. Because of this flexibility, the Robin boundary conditions are used for a huge number of problems, which can be modeled exactly by applying FEM. Furthermore, the stability, exactness, and effectiveness of FEM depend on different types of boundary conditions and also produce different types of errors and convergence of different orders. Many real-life examples can be exhibited more accurately using Neumann and Robin conditions rather than Dirichlet conditions. These types of conditions are also capable of representing various models with complex situations perfectly, which cannot be demonstrated properly by using Dirichlet conditions. Hence, it is very important to derive a simple, easier, and effective numerical method that is capable of solving such problems with Neumann and Robin conditions with higher accuracy as well as low cost within a short period of time. Consequently, in this study, we are interested in solving such PDEs with Neqmann and Robin boundary conditions by applying the FEM. To achieve this, we primarily use the FEM with two linear shape functions [23]–[26], which can handle this kind of problem faster and more accurately.

First, the generalized formulation of PDEs with mixed boundary conditions will be derived in this paper. The convergence and stability analysis of our suggested methodology will be covered in the future. In addition, calculations will be made for absolute error, dissipation error, dispersion error, and total mean square error. Three examples utilizing Dirichlet, Neumann, and Robin boundary conditions will then be included in the findings and discussion section. We'll use the derived formulation to solve them all, tabulating the results and analyzing the errors along the way. 2D and 3D graphical presentations will be added to understand the comparison between the exact and approximate results, along with maps of errors. The increased accuracy of our method will be guaranteed by this tabulated data, error analysis, and graphs. Eventually, we shall summarize our research in the following.

In the next section, we will develop the generalized formulation of PDEs with mixed boundary conditions.

2 Generalized Formulation of PDEs with Mixed Boundary Conditions

In order to derive the generalized formulation of PDEs, let's take into account a single non-linear PDE with mixed boundary conditions that looks like this:

$$\begin{cases} W_t + \sigma W W_x = \delta W_{xx} + \rho H(W(t,x)) + \mu f(x),\ t \in (0,T]\,,\ x \in D \equiv [a,b], \\ W(0,x) = W_0(x),\ x \in D, \\ \alpha_1 W(t,a) + \beta_1 \frac{\partial W}{\partial x}|_{x=a} = W_a(t),\ (t,x) \in \partial D, \\ \alpha_2 W(t,a) + \beta_2 \frac{\partial W}{\partial x}|_{x=b} = W_b(t),\ (t,x) \in \partial D. \end{cases} \tag{2.1}$$

W is the function of space (x) and time (t), or $W(t,x)$. Here, the non-linear convection term is WW_x with the coefficient, $\sigma \in \mathbb{R}$, the diffusion term is W_{xx} with diffusion coefficient, $\delta \in \mathbb{R}$, and the reaction function is $\rho H(W(t,x)) + \mu f(x)$; $\rho, \mu \in \mathbb{R}$. Then, the equation (2.1) is a non-linear convection-diffusion-reaction equation with the idea that $\rho H(W(t,x)) = W(W-1)(\beta - W)$, $0 \le \beta \le 1$. A generalized version of equation (2.1) can be obtained by declaring the trial solution (2.2).

$$\tilde{W}(t,x) = \sum_{j=1}^{n} \aleph_j(t)\theta_j(x), \tag{2.2}$$

where $\aleph_j(t)$ is the parameter representing the functions of t. Hence

$$\begin{cases} \tilde{W}_x = \sum_{j=1}^{n} \aleph_j(t) \frac{d\theta_j(x)}{dx}, \\ \tilde{W}_t = \sum_{j=1}^{n} \frac{d\aleph_j(t)}{dt} \theta_j(x). \end{cases} \tag{2.3}$$

Next, the equation for the weighted residual is,

$$\int_e \left[W_t + \sigma W W_x - \delta W_{xx} - \rho H(W(t,x)) - \mu f(x)\right] \theta_i(x) dx = 0. \tag{2.4}$$

Upon integrating by parts of equation (2.4)'s second derivative, we now obtain,

$$\delta \int_e \left[\tilde{W}_{xx}\theta_i(x)\right] dx = \delta[\tilde{W}_x\, \theta_i(x)]_e - \delta \int_e \left[\frac{d\theta_i}{dx}\tilde{W}_x\right] dx. \tag{2.5}$$

Substitute equations (2.3) and (2.5) in equation (2.4) to write the necessary equation in the standard matrix form as

$$L_{i,j}\frac{d\aleph_j(t)}{dt} + M_{i,j}\aleph_j(t) = N_i, \tag{2.6}$$

$$\text{where } L_{i,j} = \int_e \left[\sum_{j=1}^{n} \theta_j(x)\right] \theta_i(x) dx,\ \ M_{i,j} = P_{i,j} + R_{i,j},$$

$$P_{i,j} = \sigma \int_e \left[\sum_{j=1}^{n} \aleph_j(t) \frac{d\aleph_j}{dx}\theta_j(x)\right] \theta_i(x) dx + \sigma \int_e \left[\sum_{j=1}^{n} \frac{d\theta_j}{dx}\frac{d\theta_i}{dx}\right] dx,$$

$$R_{i,j} = \rho \int_e \left[\sum_{j=1}^{n} \theta_j(x)\theta_i(x)\tilde{W}^2\right] dx - \rho(\beta+1) \int_e \left[\sum_{j=1}^{n} \theta_j(x)\theta_i(x)\tilde{W}\right] dx + \rho\beta \int_e \left[\sum_{j=1}^{n} \theta_j(x)\theta_i(x)\right] dx,$$
$$N_i = \delta \left[\theta_i \tilde{W}_x\right]_e + \mu \int_e f(x)\theta_i(x)dx.$$

In this context, $L_{i,j}$ is specified as a capacity matrix, and it is comparatively easy to evaluate each of the above-mentioned matrices for each element by taking into account the two basis functions, $B_1(\varsigma)$ and $B_2(\varsigma)$, where

$$B_1(\varsigma) = \frac{(1-\varsigma)}{2},\ B_2(\varsigma) = \frac{(1+\varsigma)}{2},\ -1 \le \varsigma \le 1. \tag{2.7}$$

The first task is to divide the domain $a \le x \le b$ into a finite number of elements and compute $L_{i,j}$, $M_{i,j}$, N_i for every element. The system that results from combining those matrices is then solved using an appropriate technique to yield the solutions that are required. Now, take the n number of elements, and for the first element, $x_1 = 0$ and $x_2 = \frac{1}{n}$ and $x = x_1B_1(\varsigma) + x_2B_2(\varsigma) = 0.\frac{(1-\varsigma)}{2} + \frac{1}{n}\frac{(1+\varsigma)}{2} = 0 + \frac{(1+\varsigma)}{2n} = \frac{(1+\varsigma)}{2n} \Rightarrow dx = \frac{1}{2n}d\varsigma$. The system (2.6) can be described as follows using this relation:

$$\begin{bmatrix} L_{11}^1 & L_{12}^1 \\ L_{21}^1 & L_{22}^1 \end{bmatrix} \frac{d\aleph_j(t)}{dt} + \begin{bmatrix} P_{11}^1 + R_{11}^1 & P_{12}^1 + R_{12}^1 \\ P_{21}^1 + R_{21}^1 & P_{22}^1 + R_{22}^1 \end{bmatrix} \aleph_j(t) = \begin{bmatrix} N_1^1(t) \\ N_2^1(t) \end{bmatrix}. \tag{2.8}$$

Similarly, for second element, $x_1 = \frac{1}{n}$ and $x_2 = \frac{2}{n}$ and $x = x_1B_1(\varsigma) + x_2B_2(\varsigma) = \frac{1}{n}\frac{(1-\varsigma)}{2} + \frac{2}{n}\frac{(1+\varsigma)}{2} = \frac{1-\varsigma+2+2\varsigma}{2n} = \frac{3+\varsigma}{2n} \Rightarrow dx = \frac{1}{2n}d\varsigma$. Consequently, the system (2.6) can be displayed again as

$$\begin{bmatrix} L_{11}^2 & L_{12}^2 \\ L_{21}^2 & L_{22}^2 \end{bmatrix} \frac{d\aleph_j(t)}{dt} + \begin{bmatrix} p_{11}^2 + R_{11}^2 & P_{12}^2 + R_{12}^2 \\ P_{21}^2 + R_{21}^2 & P_{22}^2 + R_{22}^2 \end{bmatrix} \aleph_j(t) = \begin{bmatrix} N_1^2(t) \\ N_2^2(t) \end{bmatrix}. \tag{2.9}$$

Now, if we take two numbers of elements, $n = 2$, then by assembling equations (2.8) and (2.9), we obtain the following:

$$\begin{bmatrix} L_{11}^1 & L_{12}^1 & 0 \\ L_{21}^1 & L_{22}^1 + L_{11}^2 & L_{12}^2 \\ 0 & L_{21}^2 & L_{22}^2 \end{bmatrix} \frac{d\aleph_j(t)}{dt} + \begin{bmatrix} P_{11}^1 + R_{11}^1 & P_{12}^1 + R_{12}^1 & 0 \\ P_{21}^1 + R_{21}^1 & P_{22}^1 + R_{22}^1 + P_{11}^2 + R_{11}^2 & P_{12}^2 + R_{12}^2 \\ 0 & P_{21}^2 + R_{21}^2 & P_{22}^2 + R_{22}^2 \end{bmatrix} \aleph_j(t) = \begin{bmatrix} N_1^1(t) \\ N_2^1(t) + N_1^2(t) \\ N_2^2(t) \end{bmatrix}.$$

Therefore, carrying out this procedure for n number of elements and after combining them, we get the following system (2.10),

$$L\dot{W} + MW = N. \tag{2.10}$$

At this stage, discretize $\dot{W}(= \dot{\aleph}_j)$ as $\dot{W} = \frac{W_{j+1} - W_j}{\triangle t}$ and employ a particular value of time step size, $\triangle t$ and express equation (2.10) as

$$L\frac{W_{j+1} - W_j}{\triangle t} + MW_j = N,$$
$$\text{or, } LW_{j+1} + (M \triangle t - L)W_j = N \triangle t. \tag{2.11}$$

Afterwards, by imposing mixed boundary conditions in MATLAB programming and completing the row-column operation, it is possible to calculate the nodal values, W_{j+1}, at $(n+1)$ number of nodal points. For the first approximation, we will utilize the initial values that are derived from the initial condition.

3 Convergence Analysis

Let introduce the functions $B_i(\varsigma) \in \mathbb{H}_2^1$, $i = 1, 2, 3, ..., n$, where $\mathbb{H}_2^1$ stands for Hilbert space and $B_i(\varsigma)$ is representing basis functions. Also, consider the diffusion coefficients, $\delta_i, i = 1, 2$. Since $\sigma W(t, x)$, $\rho H(W(t, x))$, and $\mu f(x)$ are continuous functions, equation (2.1) has a unique solution, as shown in [7, 14]. By using the testing solution (2.2) into (2.1), the compatible matrix form (2.10) may be modified as (3.1),

$$\frac{dW_j}{dt} + L_{i,j}^{-1} M_{i,j} W_j = L_{i,j}^{-1} N_i. \tag{3.1}$$

However, it appears that equation (3.2) is an initial value problem, as shown below.

$$\begin{cases} \dfrac{dW_j}{dt} + \phi_j W_j = \iota_j, \\ W_j(0) = \zeta(\eta). \end{cases} \tag{3.2}$$

Now, the integrating factor of equation (3.2) is

$$e^{\int \phi_j dt} = e^{\phi_j t}. \tag{3.3}$$

After that, multiply (3.2) by the integrating factor (3.3) to calculate W_j over $(0, T]$. Next, we have

$$\begin{aligned} W_j e^{\phi_j t} &= \int_0^T e^{\phi_j \chi} \iota_j(\chi) d\chi, \\ \Rightarrow W_j &= \int_0^T e^{-\phi_j (t-\chi)} \iota_j(\chi) d\chi, \end{aligned}$$

and

$$|W_j|^2 \leq \frac{1}{2\phi_j} \int_0^T |\iota_j(\chi)|^2 d\chi.$$

Thus, taking a stable independent variable t, the energy norm can be written as:

$$\|\tilde{W}(t, x)\|_E^2 \leq \sum_{j=1}^{n} \frac{1}{2} \left(\int_0^T |\iota_j(\chi)|^2 d\chi \right).$$

The trial solution (2.2) is therefore convergent for a certain value of the independent variable t. The space of $(u-1)$ times continuously differentiable functions on $\overline{D}$, the closure of D, is denoted by $\mathbf{S}^{\mathbf{u},\mathbf{v}}$. A polynomial of degree at most $v-1$, where v is the number of local nodes in each element, is the restriction to D_j, $j = 0, 1, 2, ..., N-1$. For a given value of t, let $\tilde{W} \in \mathbf{S}^{\mathbf{u},\mathbf{v}}$ be the finite element solution. Then, for any $\varrho \in \mathbf{S}^{\mathbf{u},\mathbf{v}}$,

$$\left(\frac{\partial \tilde{W}}{\partial t}, \varrho \right)_0 + \Gamma \left(\tilde{W}, \varrho \right) = (\Upsilon, \varrho)_0, \tag{3.4}$$

where $\Gamma(.,.)$ and $(.,.)_0$ denote the bilinear transformation and inner product, respectively, as demonstrated in [14, 15]. In equation (3.4), the system of ordinary differential equations is substituted with an initial value problem. It is well known that, for a given t, the result will converge to the exact solution of equation (2.1) with decreasing increments in x. It is now easier to implement the iterative strategies if they show numerical stability. The stability of the iterative process, which also shows the stability of the proposed approach, will be discussed in the next section.

4 Stability Analysis

In this context, we do the stability analysis of our introduced approach since a numerically stable iteration strategy is more efficient and user-friendly. This can be accomplished by reforming equation (2.11) into the subsequent equation (4.1),

$$\{W\}_{j+1} = [\mathbb{E}] \{W\}_j + \mathbb{Q}^{-1} \{\mathbb{N}\}_j. \tag{4.1}$$

This time, the solution at time t is denoted by $\{W\}_j$, and the solution at the next generation, $(t+1)$, is denoted by $\{W\}_{j+1}$, where the next generation solution, $\{W\}_{j+1}$, depends on the current solution $\{W\}_j$. Errors may therefore be iterated. As a result of the iterative error's infinite expansion, the iterative scheme then became unstable and vice versa. The necessary and sufficient condition for the bounded error will also be

$$([\mathbb{E}] - \Lambda_{max}[I])\{W\} = 0. \tag{4.2}$$

For the eigenvalue problem (4.2), this is an unconditionally stable solution. In contrast, it will be conditionally stable when $\Lambda_{max} \leq 1$ for any time step, Δt. The following appropriate criteria are satisfied by our proposed numerical approach, which is stable.

$$\Delta t < \frac{2}{(1-2\gamma)\Lambda_{max}}; \quad \gamma < \frac{1}{2}.$$

5 Error Analysis

This part focuses on evaluating the errors of our offered numerical method, based on research by Takacs (1985) [15]. Here, the analytical and numerical solutions are denoted by E_i and A_i, which are essential to complete this calculation. Thus, the equation (5.1) provides the estimated absolute error.

$$R_{abs} = |E_k - A_k|. \tag{5.1}$$

To determine the total mean square error, our next consideration is

$$R_{tms} = \frac{1}{m}\sum_{k=1}^{m}(E_k - A_k)^2.$$

Additionally, $\delta^2(E)$ and $\delta^2(A)$ are used to represent the sample variance of the analytical and numerical solution, respectively, represented by the equation (5.2),

$$\delta^2(E) = \frac{1}{m}\sum_{k=1}^{m}(E_i - \bar{E}_i)^2, \quad \delta^2(A) = \frac{1}{m}\sum_{k=1}^{m}(A_i - \bar{A}_i)^2. \tag{5.2}$$

It is now more suitable to expand the sample variance and apply them to the concept of total mean square error. Completing a simple computation, we arrive at

$$R_{tms} = (\delta(E) - \delta(A))^2 + (\bar{E} - \bar{A})^2 + 2(1-\omega)\delta(E)\delta(A), \tag{5.3}$$

where

$$\omega = \frac{\mathrm{Cov}(E,A)}{\delta(E)\delta(A)}, \quad \mathrm{Cov}(E,A) = \frac{1}{m}\sum E_i A_i - \bar{E}\bar{A}.$$

For $\omega = 1$,

$$R_{tms} = (\delta(E) - \delta(A))^2 + (\bar{E} - \bar{A})^2.$$

After doing a mathematical inspection, we can summarize that the dispersion error and dissipation error in equation (5.3) are $2(1-\omega)\delta(E)\delta(A) = 0$ and $(\delta(E)-\delta(A))^2+(\bar{E}-\bar{A})^2$, respectively, and the following equation is working as error rate with respect to L^1 norm,

$$R_{num} = \frac{1}{m}\sum_{i=1}^{m}|E_i - A_i|.$$

6 Results and Discussion

The numerical solutions of some well-known parabolic PDEs with mixed boundary conditions are examined in this section. Along with the exact solution, all findings are shown both numerically and visually. We are using the following formula to determine absolute error [24],

$$R = |E_j^{exact} - A_j^{FEM}|.$$

Example 1. *This Example 1 is presenting a convection-diffffusion-reaction equation with Dirichlet boundary conditions. Taking* $\sigma = -1$ *and* $\delta = \rho = \mu = 1$ *into consideration, equation (2.1) transfers into equation (6.1) [13], also referred to as the Burgers-Huxley equation in one-dimensional space. In many sectors, such as biological population dynamics, fluid mechanics, and traffic flow, this equation plays a vital role to simulate convection, diffusion, and nonlinear responses in systems. It is applicable for modeling turbulence, predicting the emergence of biological patterns, and simulating automobile traffic behavior. It is also helpful in understanding complex biological and physical processes due to its ability to illustrate the balance between growth, movement, and interaction. Now, the Dirichlet boundary conditions (6.2) [13] are obtained by considering* $\alpha_1 = \alpha_2 = 1$ *and* $\beta_1 = \beta_2 = 0$ *in equation (2.1).*

$$W_t = W\,W_x + W_{xx} + W(W-1)(\beta - W);\, t \in (0,T],\, x \in D \equiv [-1,1]\,. \tag{6.1}$$

Initial and Dirichlet boundary conditions are:

$$\begin{cases} W(0,x) = P_1 - P_1 \tanh P_3 x, x \in D, \\ W(t,-1) = P_1 - P_1 \tanh\left(P_3(-1 - tP_2)\right),\, t > 0, \\ W(t,1) = P_1 - P_1 \tanh\left(P_3(1 - tP_2)\right),\, t > 0, \end{cases} \tag{6.2}$$

where $P_1 = \frac{\beta-1}{2}$; $P_2 = \frac{\beta+1}{2}$ *and* $P_3 = \frac{\beta-1}{4}$. *In this Example 1, take* $\beta = 0.00001$ *and the theoretical solution corresponding to (6.1) [13] can be written as*

$$W(t,x) = P_1 - P_1 \tanh\left(P_3(x - tP_2)\right);\, t \in (0,T],\, x \in D.$$

Applying the weak formulation of FEM with linear shape functions (2.7), derived in Section 2, we now obtain the compatible matrix form (2.6). The following exhibit the capacity matrix, L_{ij}, stiffness matrix, M_{ij}, and load vector, $N_i(t)$:

$$\begin{cases} L_{i,j} = \int\limits_e \left[\sum\limits_{j=1}^{n} \theta_j(x)\right] \theta_i(x) dx, \\ M_{i,j} = P_{i,j} - R_{i,j},\ P_{i,j} = \int\limits_e \dfrac{d\theta_i}{dx} \left[\sum\limits_{j=1}^{n} \dfrac{d\theta_j(x)}{dx}\right] dx, \\ R_{i,j} = \int_e \left[\sum\limits_{j=1}^{n} \left(1.00001\tilde{W}^2 - 0.00001\tilde{W} - \tilde{W}^3\right)\right] \theta_i(x) dx, \\ N_i(t) = [\tilde{W}_x \theta_i(x)]_e. \end{cases}$$

After carrying out a fundamental calculation, the required final system is

$$LW_{j+1} + (M \triangle t - L)W_j = N \triangle t.$$

Taking two linear shape functions (2.7) and a limited number of elements ($n = 10$) with $n+1 = 11$ nodal points, we proceed to the last step. The estimated solution, W_{j+1}, is then obtained from this system by using the row-column operation. Here, we have applied initial and Dirichlet boundary conditions (6.2) [13] in MATLAB programming to finish this numerical computation. Table 6.1 then provides the necessary outcomes.

Table 6.1: FEM and theoretical solution of equation (6.1) at various time steps, $h = \Delta t$.

x	$h = \Delta t = 10^{-4}$			$h = \Delta t = 10^{-3}$			$h = \Delta t = 10^{-2}$		
	FEM	Exact	*Error*	FEM	Exact	*Error*	FEM	Exact	*Error*
-1.0	-0.3776	-0.3775	1.0×10^{-04}	-0.3779	-0.3775	1.0×10^{-03}	-0.3808	-0.3770	1.0×10^{-02}
-0.8	-0.4013	-0.4013	6.3×10^{-06}	-0.4012	-0.4012	6.3×10^{-05}	-0.4005	-0.4007	6.3×10^{-04}
-0.6	-0.4256	-0.4255	2.0×10^{-05}	-0.4256	-0.4255	2.0×10^{-04}	-0.4258	-0.4249	2.0×10^{-03}
-0.4	-0.4502	-0.4502	1.3×10^{-05}	-0.4502	-0.4501	1.3×10^{-04}	-0.4501	-0.4495	1.2×10^{-03}
-0.2	-0.4750	-0.4750	1.4×10^{-05}	-0.4750	-0.4750	1.4×10^{-04}	-0.4750	-0.4744	1.4×10^{-03}
0.0	-0.5000	-0.5000	1.3×10^{-05}	-0.4999	-0.4999	1.3×10^{-04}	-0.4999	-0.4994	1.3×10^{-03}
0.2	-0.5250	-0.5250	1.2×10^{-05}	-0.5250	-0.5249	1.2×10^{-04}	-0.5250	-0.5244	1.2×10^{-03}
0.4	-0.5498	-0.5498	1.2×10^{-05}	-0.5498	-0.5498	1.2×10^{-04}	-0.5450	-0.5492	1.2×10^{-03}
0.6	-0.5744	-0.5744	6.3×10^{-06}	-0.5744	-0.5744	6.3×10^{-05}	-0.5742	-0.5738	6.3×10^{-04}
0.8	-0.5987	-0.5987	2.4×10^{-05}	-0.5988	-0.5986	2.4×10^{-04}	-0.5995	-0.5981	2.4×10^{-03}
1.0	-0.6224	-0.6224	4.3×10^{-05}	-0.6221	-0.6224	4.3×10^{-04}	-0.6192	-0.6219	4.3×10^{-03}

Table 6.2: Error analysis of FEM solutions of equation (6.1).

h	E_{num}	Dissipation Error	Dispersion Error	Total Error
10^{-4}	2.4117×10^{-05}	9.7959×10^{-11}	1.4938×10^{-10}	2.4734×10^{-10}
10^{-3}	2.4120×10^{-04}	9.7823×10^{-09}	1.495×10^{-08}	2.4734×10^{-08}
10^{-2}	2.4148×10^{-03}	9.6458×10^{-07}	1.5087×10^{-06}	2.4732×10^{-06}

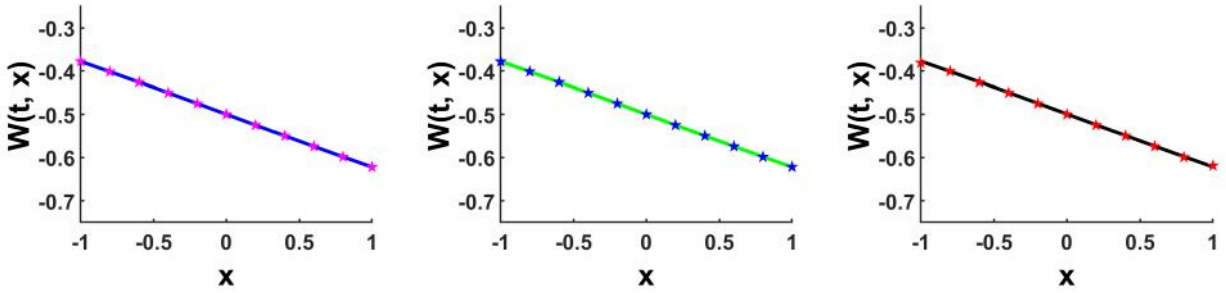

Figure 6.1: Comparative analysis of theoretical and FEM approximations of equation (6.1) at different time steps, $h = \Delta t$.

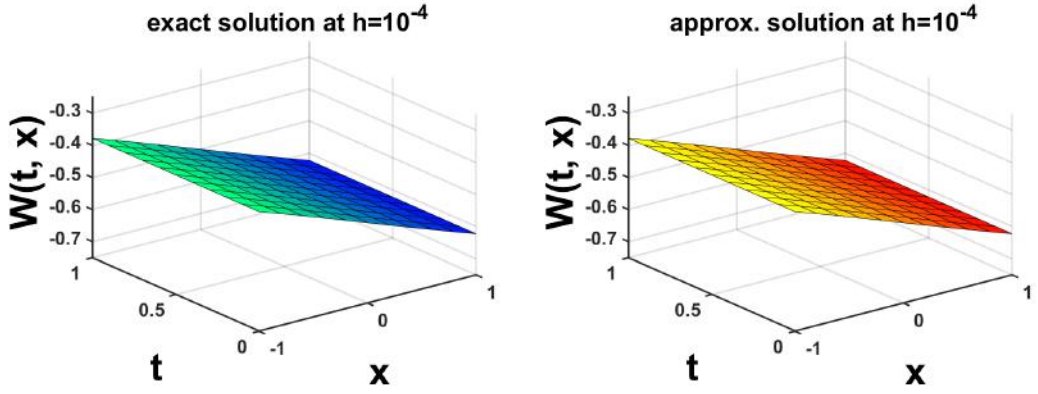

Figure 6.2: Theoretical solutions and FEM approximations of equation (6.1) at $h = 10^{-4}$.

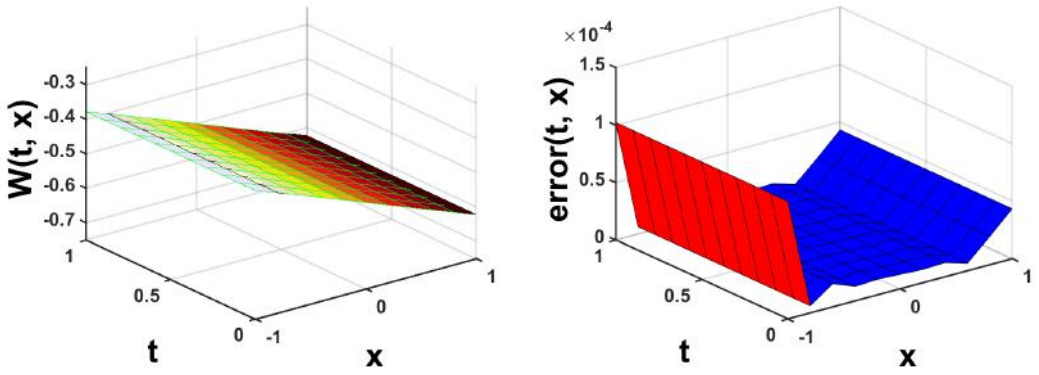

Figure 6.3: Comparison between theoretical and approximate solutions of equation (6.1) at $h = 10^{-4}$ with error map.

Table 6.1 shows that, by considering different time steps ($h = \Delta t$) for the equation (6.1), our numerical scheme that we developed performs more accurately over the spatial domain x. Interestingly, we find good agreement between the properties of the theoretical and approximation solutions. Additionally, Table 6.2 illustrates many error types, including total mean square error, dissipation error, and dispersion error. They're all more accurate than our thought-out strategy. Graphical representations of the data acquired using our developed formulation are shown in Figure 6.1 at different time steps ($h = \Delta t$). This image shows the correctness and acceptability of our numerical scheme by clarifying the correspondence between the exact and approximation solutions at various time steps ($h = \Delta t$). Observing the tabulated data and graphical presentation, we have found that the result will be more accurate for smaller time steps. Figure 6.2 is showing the three-dimensional surface plots of equation (6.1) at the time step $h = 10^{-4}$, which is more transparent to understand the accuracy of our introduced method. Also, Figure 6.3 is presenting the comparative study between exact and approximate solutions through 3D surface plots and error analysis at $h = 10^{-4}$. This comparative study and error map ensure the acceptance and efficacy of this method, highlight the fast convergence and stability of the FEM, and validate its application in solving different PDEs with Dirichlet boundary conditions as well as nonlinear CDR equations with Dirichlet boundary conditions.

Example 2. *In this instance, let introduce a diffusion-reaction equation with Neumann boundary conditions. Take $\sigma = 0, \delta = \rho = \mu = 1$ in equation (2.1) to deduce this desired equation. As a result, we obtain the equation (6.3) [22] that has $H(W(t,x)) = \frac{\pi^2}{2} e^{\frac{-\pi^2}{2}t} \cos(\pi x)$ and $f(x) = x - 2$. Equation (2.1) yields this equation (6.3) with Neumann boundary conditions (6.4) [22] by considering $\alpha_1 = \alpha_2 = 0, \beta_1 = \beta_2 = 1, W_0(t) = t, W_1(t) = 2+t$, and so forth.*

$$W_t = W_{xx} + \frac{\pi^2}{2} e^{\frac{-\pi^2}{2}t} \cos(\pi x) + x - 2;\ t \in (0, T],\ x \in D \equiv [0, 1]\,. \tag{6.3}$$

Initial and Neumann boundary conditions are:

$$\begin{cases} W(0,x) = x^2 + \cos(\pi x), x \in D, \\ \frac{\partial W}{\partial x}|_{x=0} = t,\ t > 0, \\ \frac{\partial W}{\partial x}|_{x=1} = 2 + t,\ t > 0, \end{cases} \tag{6.4}$$

The corresponding exact solution is $W(t,x) = x^2 + xt + e^{-\frac{\pi^2}{2}t} \cos(\pi x)$, $t \in (0, T]$, $x \in D$.

Similar to Example 1, we utilize the expanded FEM formulation for the PDEs with Neumann boundary conditions, using linear shape functions. Therefore, it is possible to obtain the appropriate matrix form (2.6) where

$$\begin{cases} L_{i,j} = \int\limits_e \left[\sum\limits_{j=1}^{n} \theta_j(x)\right] \theta_i(x) dx,\ M_{i,j} = \int\limits_e \left[\sum\limits_{j=1}^{n} \frac{d\theta_j}{dx} \frac{d\theta_i}{dx}\right] dx, \\ N_i = \left[\theta_i(x) \frac{\partial \bar{W}}{\partial x}\right]_e + \int\limits_e \frac{\pi^2}{2} e^{\frac{-\pi^2}{2}t} \cos(\pi x) \theta_i(x) dx + \int\limits_e (x-2)\theta_i(x) dx. \end{cases}$$

After completing the above mentioned simplification, we get the following system,

$$LW_{j+1} + (M \triangle t - L)W_j = N_i \triangle t.$$

We now employ row-column operation to get the estimated FEM solutions, W_{j+1}, from this system by applying initial and Neumann boundary conditions in MATLAB programming. Here, $n = 10$ number of elements with 11 nodal points and two linear shape functions (2.7) are utilized. Therefore, Table 6.3 tabulates the approximate solutions that are produced.

Table 6.3: FEM and precise solution of equation (6.3) at different time steps, $h = \Delta t$.

x	$h = \Delta t = 10^{-4}$			$h = \Delta t = 10^{-3}$			$h = \Delta t = 10^{-2}$		
	FEM	Exact	*Error*	FEM	Exact	*Error*	FEM	Exact	*Error*
0.0	1.0000	0.9990	1.0×10^{-03}	1.0000	0.9902	9.8×10^{-03}	0.9998	0.9060	9.3×10^{-02}
0.1	0.9611	0.9601	9.0×10^{-04}	0.9610	0.9518	9.2×10^{-03}	0.9609	0.8727	8.8×10^{-02}
0.2	0.8490	0.8482	8.0×10^{-04}	0.8490	0.8413	7.7×10^{-03}	0.8489	0.7750	7.3×10^{-02}
0.3	0.6778	0.6772	5.0×10^{-04}	0.6778	0.6723	5.5×10^{-03}	0.6777	0.6255	5.2×10^{-02}
0.4	0.4690	0.4688	3.0×10^{-04}	0.4690	0.4664	2.6×10^{-03}	0.4690	0.4440	2.5×10^{-02}
0.5	0.2500	0.2501	0.0×10^{-04}	0.2500	0.2505	5.0×10^{-04}	0.2501	0.2550	5.0×10^{-03}
0.6	0.0510	0.0513	4.0×10^{-04}	0.0510	0.0546	3.6×10^{-03}	0.0511	0.0860	3.5×10^{-02}
0.7	-0.0978	-0.0971	6.0×10^{-04}	-0.0978	-0.0913	6.4×10^{-03}	-0.0976	-0.0355	6.2×10^{-02}
0.8	-0.1690	-0.1681	9.0×10^{-04}	-0.1690	-0.1603	8.7×10^{-03}	-0.1689	-0.0850	8.4×10^{-02}
0.9	-0.1410	-0.1400	1.0×10^{-03}	-0.1410	-0.1308	1.0×10^{-02}	-0.1403	-0.0427	9.7×10^{-02}
1.0	-0.0000	0.0011	1.1×10^{-03}	-0.0001	0.0108	1.1×10^{-02}	-0.0014	0.1040	1.0×10^{-01}

Table 6.4: Error analysis of FEM solutions of equation (6.3).

h	E_{num}	Dissipation Error	Dispersion Error	Total Error
10^{-4}	6.8725×10^{-04}	5.4826×10^{-07}	3.1559×10^{-08}	5.7981×10^{-07}
10^{-3}	6.8000×10^{-03}	5.4316×10^{-05}	3.1764×10^{-06}	5.7492×10^{-05}
10^{-2}	6.5600×10^{-02}	4.9000×10^{-03}	3.4110×10^{-04}	5.3000×10^{-03}

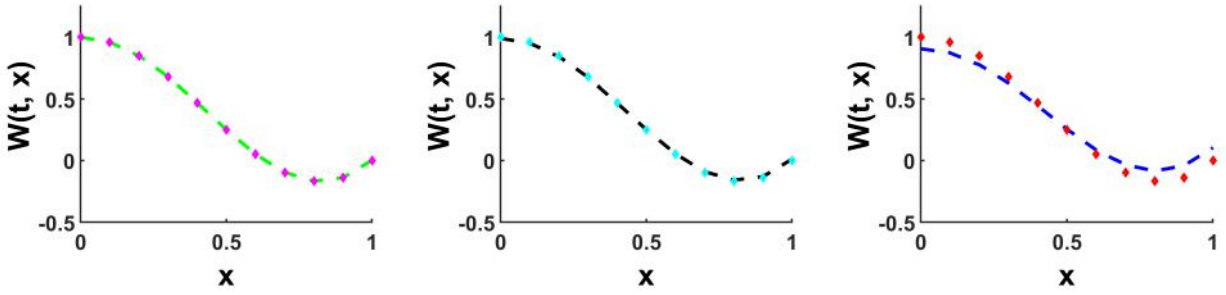

Figure 6.4: FEM and precise solutions of equation (6.3) at three different time steps, $h = \Delta t$.

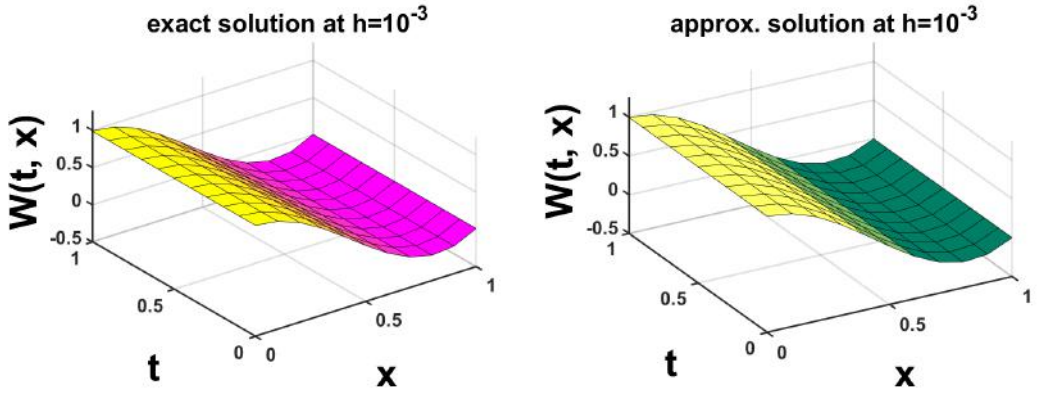

Figure 6.5: Precise and FEM solutions of equation (6.3) at $h = 10^{-3}$.

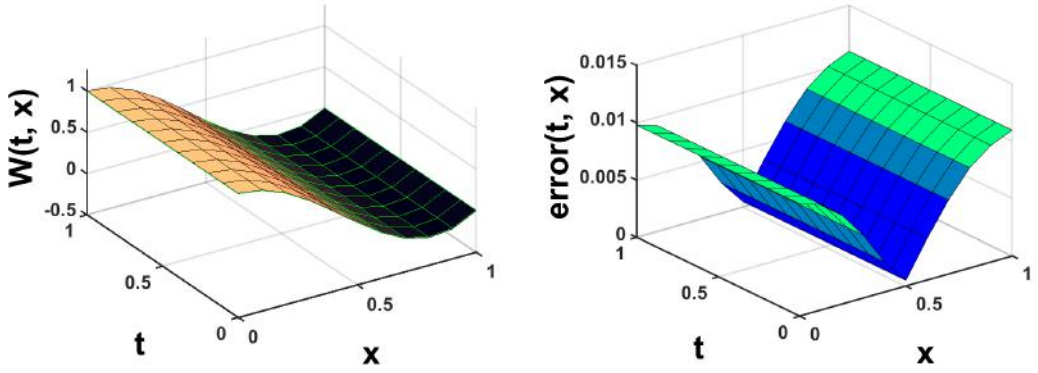

Figure 6.6: Correlation between precise and FEM solutions of equation (6.3) at $h = 10^{-3}$ and an error map.

At this point, we can make sure that there is a well-ordered harmony between the exact and approximate solutions of equation (6.3) at various time steps, $h = \Delta t$, by looking at Tables 6.3 and 6.4. Table 6.3 shows the tabulated data, while Table 6.4 shows the various kinds of errors. Figure 6.4 exhibits the comparative analysis of precise and approximate solutions graphically. For getting a transparent idea, surface plots of exact and approximate solutions are presented in Figure 6.5 at the time step, $h = 10^{-3}$. The error map and correlative study in 3D between the exact and approximate solutions of equation (6.3) are displayed in Figure 6.6. After completing a careful review, we may summarize that the combined tabular data and graphical displays verify the convergence, stability, accuracy, and acceptance of our approach for solving a class of parabolic PDEs with Neumann boundary conditions as well as CDR equations.

Example 3. *In this study, our main goal is to solve parabolic PDEs as well as CDR equations with mixed boundary conditions. Two cases involving Dirichlet and Neumann boundary conditions have already been resolved. The remaining criteria are now Robin boundary conditions, and we use the uniformly propagating shock problem with Robin boundary conditions in this case. Uniformly propagating shock problems have importance in the field of aerospace engineering, where they aid in the design of supersonic aircraft, and in the field of medical procedures like lithotripsy, which breaks kidney stones using shock waves. Predicting natural calamities such as tsunamis and streamlining high-energy reaction-based industrial operations both are dependable on an understanding of shock dynamics. Shock propagation also facilitates innovations in technology, safety, and public health, which also develop numerical methodologies. Now, consider* $\sigma = 1, \delta = \frac{1}{Re}$ *where* $1 \leq Re \leq 10^5, \rho = 0, \mu = 0$ *and* $\alpha_1 = \alpha_2 = \beta_1 = 1, \beta_2 = -1$ *in equation (2.1), which converts equation (2.1) into a convection-diffusion equation named as the uniformly propagating shock problem (6.5) [7],*

$$W_t + WW_x = \frac{1}{Re} W_{xx}; t \in (0, T] \equiv (0, 1], \, x \in D \equiv [-1, 1]. \tag{6.5}$$

Initial and Robin boundary conditions [7] are:

$$\begin{cases} W(0,x) = \frac{x-4}{x-2},\ x \in D, \\ W(t,-1) + \frac{\partial W}{\partial x}|_{x=-1} = W_1(t),\ t > 0, \\ W(t,1) + \frac{\partial W}{\partial x}|_{x=1} = W_2(t),\ t > 0, \end{cases} \tag{6.6}$$

with $Re = 10^4, W_1(t) = \frac{t^2+8T+13}{(t+3)^2}$ *and* $W_2(t) = \frac{t^2+4T+5}{(t+1)^2}$ *and the analytical solution is* $W(t,x) = 1 - \frac{2}{x-t-2}, t \in (0,T]\ ,\ x \in [-1,1]$.

The FEM approximation for equation (6.5) [7] is obtained by applying the generalized formulation derived in Section 2, just like in the preceding two examples. Hence, the matrix form (2.6) is obtained with the following:

$$\begin{cases} L_{i,j} = \int\limits_e \left[\sum\limits_{j=1}^{n} \theta_j(x)\right] \theta_i(x)dx,\ M_{i,j} = P_{i,j} + R_{i,j}, \\ P_{i,j} = \aleph_1(t) \int\limits_e \left[\sum\limits_{j=1}^{n} \theta_j(x)\right] \theta_i(x)\frac{d\theta_1}{dx}dx + \aleph_2(t) \int\limits_e \left[\sum\limits_{j=1}^{n} \theta_j(x)\right] \theta_i(x)\frac{d\theta_2}{dx}dx, \\ R_{i,j} = \frac{1}{Re} \int\limits_e \left[\sum\limits_{j=1}^{n} \frac{d\theta_j}{dx}\right] \frac{d\theta_i}{dx}dx,\ N_i = \frac{1}{Re}\left[\theta_i(x)\frac{\partial \tilde{W}}{\partial x}\right]_e. \end{cases}$$

Simplify the above mentioned computation to obtain the suitable system that follows:

$$LW_{j+1} + (M \triangle t - L)W_j = N_i \triangle t.$$

Using the row-column operation with $n = 10$ number of elements, the approximate solution, W_{j+1}, is now obtained from this system. It is important to note that the row-column operation and above simplification in this study were carried out by imposing initial and Robin boundary conditions (6.6) [7] in MATLAB programming. There is a tabulation of the approximate solutions generated in Table 6.5.

Table 6.5: FEM and analytical solutions of equation (6.5) at various time steps, $h = \Delta t$.

x	$h = \Delta t = 10^{-4}$			$h = \Delta t = 10^{-3}$			$h = \Delta t = 10^{-2}$		
	FEM	Exact	*Error*	FEM	Exact	*Error*	FEM	Exact	*Error*
-1.0	1.6667	1.6666	1.8×10^{-05}	1.6666	1.6664	2.0×10^{-04}	1.6663	1.6645	1.8×10^{-03}
-0.8	1.7143	1.7143	2.1×10^{-05}	1.7142	1.7140	2.0×10^{-04}	1.7139	1.7117	2.1×10^{-03}
-0.6	1.7692	1.7692	2.5×10^{-05}	1.7692	1.7689	3.0×10^{-04}	1.7688	1.7663	2.5×10^{-03}
-0.4	1.8333	1.8333	3.0×10^{-05}	1.8333	1.8330	3.0×10^{-04}	1.8329	1.8299	3.0×10^{-03}
-0.2	1.9091	1.9090	3.6×10^{-05}	1.9090	1.9087	4.0×10^{-04}	1.9086	1.9050	3.7×10^{-03}
0.0	2.0000	2.0000	4.5×10^{-05}	2.0000	1.9995	5.0×10^{-04}	1.9995	1.9950	4.5×10^{-03}
0.2	2.1111	2.1110	5.6×10^{-05}	2.1111	2.1105	6.0×10^{-04}	2.1106	2.1050	5.6×10^{-03}
0.4	2.2500	2.2500	7.3×10^{-05}	2.2499	2.2492	7.0×10^{-04}	2.2495	2.2422	7.2×10^{-03}
0.6	2.4286	2.4285	9.6×10^{-05}	2.4285	2.4276	1.0×10^{-03}	2.4280	2.4184	9.6×10^{-03}
0.8	2.6667	2.6665	1.3×10^{-04}	2.6666	2.6653	1.3×10^{-03}	2.6660	2.6529	1.3×10^{-02}
1.0	3.0000	2.9998	1.9×10^{-04}	2.9999	2.9980	1.9×10^{-03}	2.9993	2.9802	1.9×10^{-02}

Table 6.6: Error analysis of FEM solutions of equation (6.5).

h	E_{num}	Dissipation Error	Dispersion Error	Total Error
10^{-4}	6.62289×10^{-05}	$7.0552\ \times10^{-09}$	$6.1322\ \times10^{-11}$	7.1165×10^{-09}
10^{-3}	6.6183×10^{-04}	$7.0440\ \times10^{-07}$	$6.1178\ \times10^{-09}$	7.1052×10^{-07}
10^{-2}	6.6000×10^{-03}	6.9337×10^{-05}	5.9723×10^{-07}	6.9935×10^{-05}

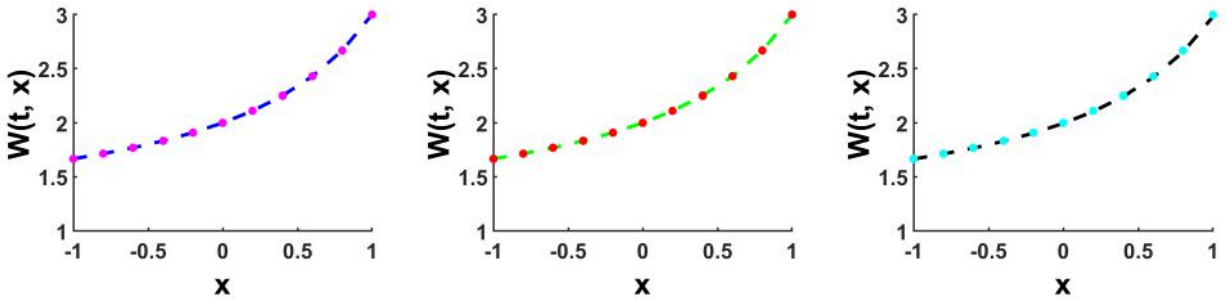

Figure 6.7: An analysis comparing the analytic and FEM solutions of equation (6.5) at various time steps, $h = \Delta t$.

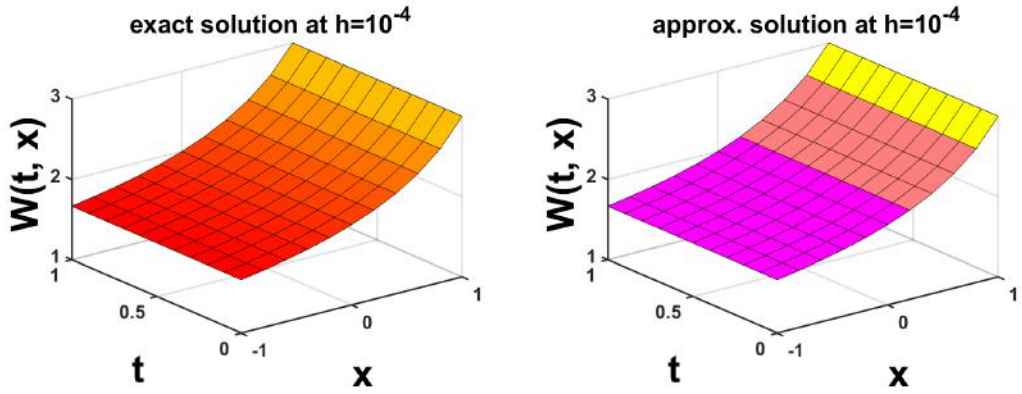

Figure 6.8: Analytic and FEM solutions of equation (6.5) at $h = 10^{-4}$.

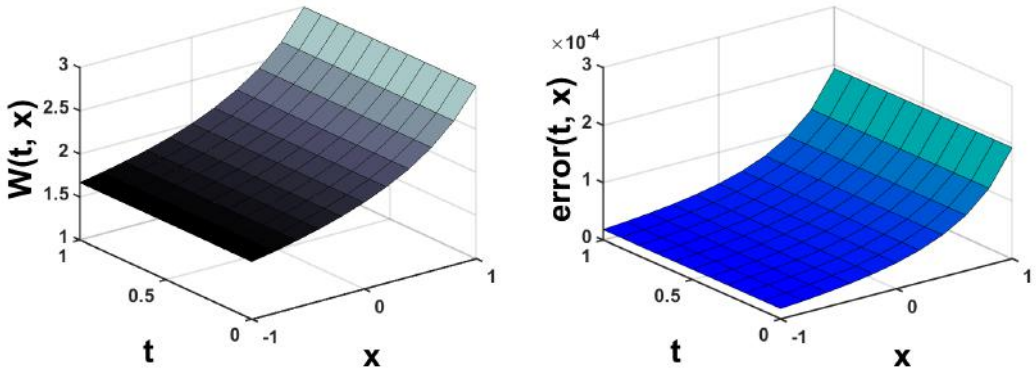

Figure 6.9: Correlation between analytic and FEM solutions of equation (6.5) at $h = 10^{-4}$ with error map.

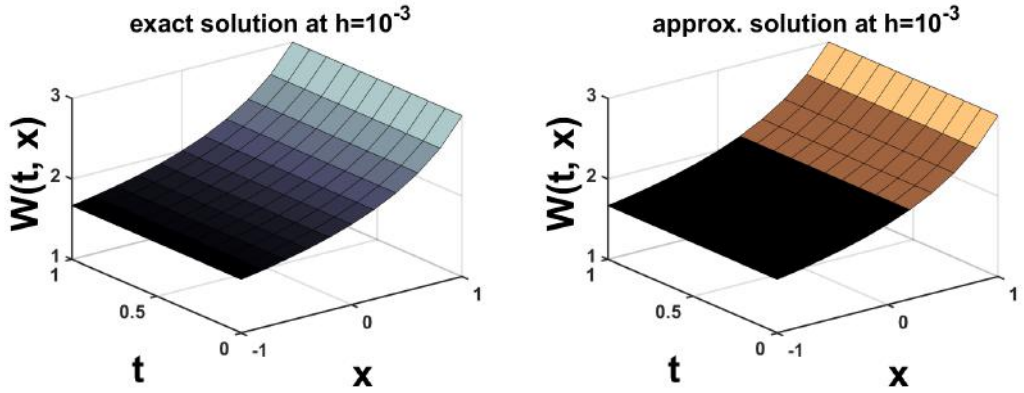

Figure 6.10: Analytic and FEM solutions of equation (6.5) at $h = 10^{-3}$.

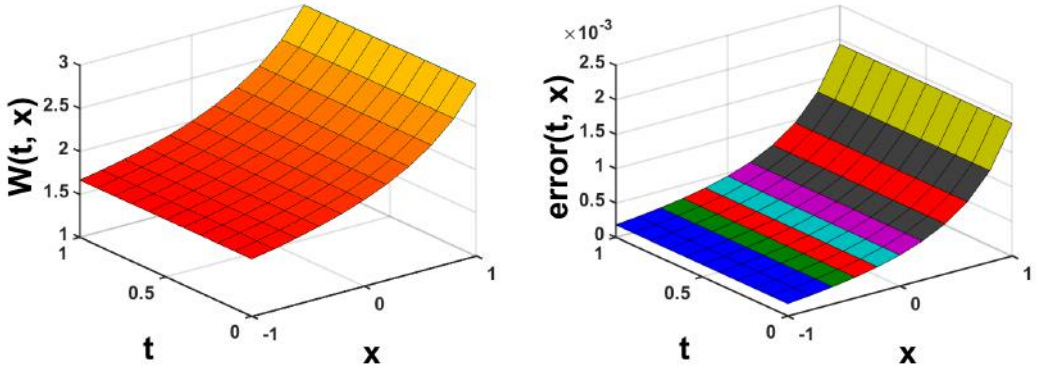

Figure 6.11: Correlation between analytic and FEM solutions of equation (6.5) at $h = 10^{-3}$ and an error map.

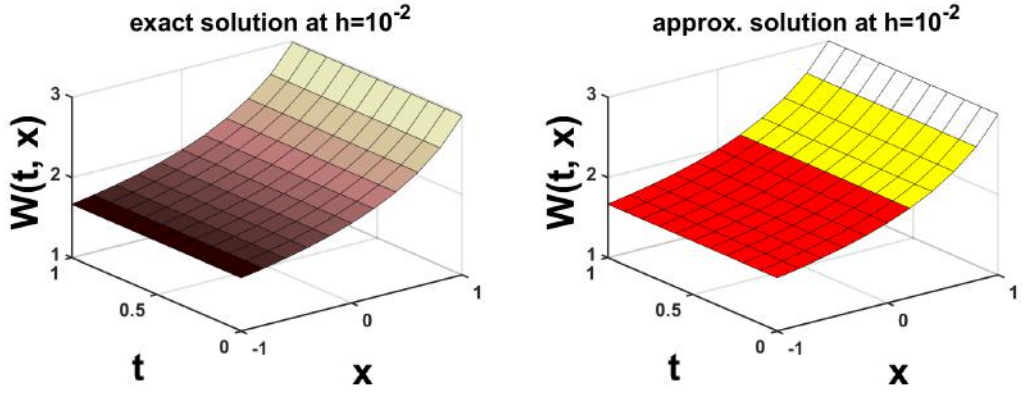

Figure 6.12: Analytic and FEM solutions of equation (6.5) at $h = 10^{-2}$.

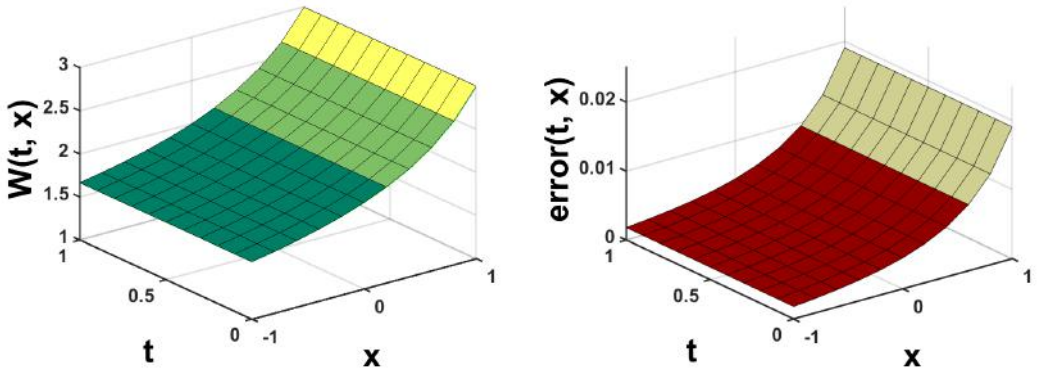

Figure 6.13: Correlation between analytic and FEM solutions of equation (6.5) at $h = 10^{-2}$ and an error map.

The accuracy of our approach method for the uniformly propagating shock problem with Robin boundary conditions is comparatively good for smaller time increments $h = \Delta t$, according to a detailed study of the data in Table 6.5. The analysis of different kinds of errors, including dissipation error, dispersion error, total mean square error etc., is displayed in Table 6.6. The FEM solutions and the analytical solutions of equation (6.5) have been shown to be closely related. These outcomes further validate the precision and effectiveness of our methodology. Furthermore, we have included a graphical comparison in Figure 6.7 between the numerical and analytic solutions of equation (6.5). For a deeper comprehension of the accuracy of this approach, 3D surface plots of both solutions to equation (6.5) are then provided here (see Figures 6.8, 6.10, and 6.12). Additionally, Figures 6.9, 6.11, and 6.13, which offer a correlative study between both solutions of equation (6.5) and error map at various time steps, illustrate the convergence, stability, and correctness of our methodology for solving PDEs as well as convection-diffusion equations with Robin boundary conditions.

7 Conclusion

There are numerous significant fields in which non-linear PDEs and CDR equations with mixed boundary conditions are used. In this study, we focused on using FEM with linear shape functions to obtain more accurate numerical solutions for them. Initially, we reviewed some literature to understand the research significance of this topic. Then, we formulated the weighted residual equation and derived the generalized weak formulation of our approach for non-linear PDEs with Dirichlet, Neumann, and Robin boundary conditions. After that, we included two effective sections: convergence analysis and stability analysis of this method in our study, which explain the convergence and stability of our approach. To understand the accuracy of this approach, the error analysis section has also been added, where the absolute error, dissipation error, dispersion error, and total mean square error are discussed. The next result and discussion section has contained three examples. Among them, the first is a nonlinear CDR equation with Dirichlet boundary conditions, the second is a diffusion-reaction equation with Neumann boundary conditions, and the last is a uniformly propagating shock problem with Robin boundary conditions. The accuracy and effectiveness of this approach have been proven by tabulated data, a graphical depiction of each case at different time steps $h = \Delta t$, and omittable errors presented by Tables 6.2, 6.4, and 6.6. Based on the reasoning above, our method is convergent, stable, and offers higher-order accuracy. In conclusion, our method's affordability, simplicity, ease of formulation, time-saving qualities, and compatibility with the actual solution in the whole one-dimensional space make it effective, accurate, and generally recognized for both PDEs and CDR equations with mixed boundary conditions.

Acknowledgements

The authors express their gratitude to the anonymous referees and editor for their insightful feedback and this research was partially supported by the Noakhali Science and Technology University Research Cell (NSTURC).

References

[1] P. E. Lewis, and J. P. Ward, The Finite Element Method (Principles and Applications), *Wokingham: Addison-Wesley*, (1991).

[2] Y. W. Kwon, and H. Bang, The Finite Element Method Using Matlab, *Mechanical and Aerospace Engineering Series, CRC Press*, (2000).

[3] C. Zhangxin, Finite Element Methods and Their Applications, *Springer Science and Business Media*, (2005).

[4] S. S. Rao, The Finite Element Method in Engineering, *Elsevier*, (2010).

[5] J.N. Reddy, An Introduction to Nonlinear Finite Element Analysis, *Oxford University Press*, (2004).

[6] J. F. Neville, X. Jingyu, and Y. Yubin, A Finite Element Method for Time Fractional Partial Differential Equations, *Fract. Calc. Appl. Anal.*, 14, 454–474 (2011).

[7] H. Ali, and M. Kamrujjaman, Numerical Solutions of Nonlinear Parabolic Equations with Robin Condition: Galerkin approach, *TWMS Journal of Applied and Engineering Mathematics*, 12(3), 851-863 (2022).

[8] H. Ali, M. Kamrujjaman, and M. S. Islam, An Advanced Galerkin Approach to Solve the Nonlinear Reaction-Diffusion Equations With Different Boundary Conditions, *Journal of Mathematics Research*, 14(1), 30-45 (2022).

[9] H. Ali, T. Datta, and M. Kamrujjaman, Efficient Family of Iterative Methods for Solving Nonlinear Simultaneous Equations: A comparative Study, *Journal of Applied Mathematics and Computation*, 5(4), 331–337 (2021).

[10] H. Ali, M. Kamrujjaman, and A. Shirin, Numerical Solution of a Fractional Order Bagley-Torvik Equation by Quadratic Finite Element Method, *Journal of Applied Mathematics and Computing*, 1–17 (2020).

[11] H. Ali, M. Kamrujjaman, and M. S. Islam, Numerical Computation of FitzHugh-Nagumo Equation: A Novel Galerkin Finite Element Approach, *International Journal of Mathematical Research*, 9(1), 20–27 (2020).

[12] J.E. Macías-Díaz, and A.E. González, A Convergent and Dynamically Consistent Finite-Difference Method to Approximate the Positive and Bounded Solutions of the Classical Burgers–Fisher Equation, *Journal of Computational and Applied Mathematics*, 0377-0427 (2015).

[13] M. Saqib et al., A Computational Analysis to Burgers Huxley Equation, *Computers, Materials and Continua*, (2020).

[14] I. Babuska, and A. K. Aziz, Survey Lectures on the Mathematical Foundation of the Finite Element Method, In: A. K. Aziz, Ed., The Mathematical Foundations of the Finite Element Method with Applications to Partial Differential Equations, *Academic Press, New York*, 3-359 (1972).

[15] I. Babuska, and W. C. Rheinboldt, Error Estimates for Adaptive Finite Element Computations, *SIAM J. on Numerical Analysis*, 15(4), 736-754 (1978).

[16] I. Babuska, and W. C. Rheinboldt, A Posteriori Error Estimates for the Finite Element Method, *International Journal for Numerical Methods in Engineering*, 12, 1597-1615 (1978).

[17] C. Takacs, A Two-Step Scheme for the Advection Equation with Minimised Dissipation and Dispersion Errors, *A Monthly Weather Review*, 113, 1050–1065 (1985).

[18] N. Mphephu, Numerical Solution of 1-D Convection-Diffusion-Reaction Equation, *MSc Thesis, University of Venda, African Institute for Mathematical Sciences*, (2013).

[19] A. Singh et al., Numerical Solution of Burgers–Huxley Equation Using a Higher Order Collocation Method, *Journal of Mathematics*, (2024).

[20] A. G. Kushner and R. I. Matviichuk, Exact solutions of the Burgers–Huxley Equation Via Dynamics, *Journal of Geometry and Physics*, 151, 103615 (2020).

[21] M. Yiğider, M. Karabacak, The Numerical Solution of Helmholtz Equation Via Multivariate Padé Approximation, *International Journal of Research in Engineering and Technology*, 2321-7308 (2014).

[22] A. Cheniguel, A Numerical Method for the Heat Equation with Dirichlet and Neumann Conditions, *Proceedings of the International MultiConference of Engineers and Computer Scientists*, 1, 12–14 (2014).

[23] S. A. Lima, M. Kamrujjaman, and M. S. Islam, Direct Approach to Compute a Class of Reaction-Diffusion Equation by a Finite Element Method, *Journal of Applied Mathematics and Computation*, 4(2), 26–33 (2020).

[24] S. A. Lima, M. Kamrujjaman, and M. S. Islam, Numerical Solution of Convection-Diffusion-Reaction Equations by a Finite Element Method with Error Correlation, *AIP Advances*, 11(8), (2021).

[25] S. A. Lima and F. Khondaker, A Finite Element Method for Numerical Solution of Parabolic Diffusion-Reaction Equation, *GANIT: Journal of Bangladesh Mathematical Society*, Soc. 42.2, 14-23 (2022).

[26] S. A. Lima et al., Numerical Method to Solve Generalized Nonlinear System of Second-order Boundary Value Problems: Galerkin Approach, *Advances in the Theory of Nonlinear Analysis and its Applications*, 7(20), 280-291 (2023).